An Implementation of the Average Atom Model using the Thermodynamic Consistency Condition: Application to Ar

F. Lanzini[a,b,c,*] and H.O. Di Rocco[a,b,d]

[a]Departamento de Cs. Físicas y Ambientales, Fac. Cs. Exactas,
Universidad Nacional del Centro de la Provincia de Buenos Aires, Pinto 399 (7000), Tandil, Argentina
[b]Consejo Nacional de Investigaciones Científicas y Técnicas (CONICET), Argentina
[c]Instituto de Física de Materiales Tandil (IFIMAT), Argentina
[d]Centro de Investigaciones en Física e Ingeniería del Centro de la Provincia de Buenos Aires (CIFICEN), Argentina

(Received March 22, 2018; in final form October 28, 2018)

We present a computational implementation of the average atom model for the calculation of matter properties under different conditions of density and temperature. Different issues related to the practical implementation, particularly those concerning the choice of an energy value acting as a boundary between free and bound electron states are discussed. As a test case, the ionization degree, electron density, and contributions to the potential $V(r)$ are computed for Ar at temperatures ranging from a few eV to some keV, and ionic densities between 1×10^{19} cm^{-3} and 1×10^{23} cm^{-3}. Results of the model are compared with those obtained by means of the Thomas–Fermi model and by other analytical approaches.

DOI: 10.12693/APhysPolA.134.1126
PACS/topics: 31.15.bt, 52.25.Jm, 52.27.Aj

1. Introduction

The interest in the study of warm and dense matter (WDM) properties is related to advanced energy technologies, the study of astrophysical objects, laser-produced plasma in inertial confinement fusion and X-ray lasers [1, 2]. For the study of WDM, the distribution of ionic species and excited state populations need to be calculated. In cases where the number of configurations to be considered is large (for instance, for high Z plasmas), it turns difficult to accurately solve the relevant equations [3, 4]. In these cases, an alternative approach is the average atom model (AAM). Instead of dealing with multiple different configurations, the AAM treats a single, average ion, with non integer populations, given by the Fermi–Dirac statistics. The AAM is widely employed for the calculation, for instance, of equations-of-state (EOS) and opacity properties [5].

Different variants of the AAM exist, and most of them are based on the ion-sphere (IS) model [6]. In this approach, the space occupied by a plasma with ionic density n_i is subdivided into spherical cells (also called the Wigner–Seitz cells) of radius $R_0 = (3/4\pi n_i)^{1/3}$. Within the sphere there is a nucleus of charge Z together with Z surrounding electrons, in such a way that the ion cell as a whole is neutral. The nucleus is supposed to be fixed at the center of the ion-sphere, and the electrons are distributed according to an electron density $\rho(r)$. Since $\rho(r)$ determine the potential $V(r)$ in which the electrons move, the problem is self-consistent. Different approaches to the AAM differ, among other details, in the way in which they obtain the electron density. For instance, the generalization of the Thomas–Fermi (TF) model [7, 8] to non-zero temperatures [9] is a particular case of IS-AAM in which no distinction is made between bound and free electrons, giving to all of them a semi-classical treatment [10]. Refinements of this model can be obtained by treating separately bound and free electrons, including exchange terms in the potential, etc.

In this work, we present an implementation of the AAM based on the relativistic Hartree–Fock–Slater (RHFS) model as described by Nikiforov and coworkers in [11, 12]. In this implementation, the bound electrons are treated quantum mechanically, and the free electrons in a semiclassical way. The value of the energy ϵ_0 separating the bound and the free electrons (the effective boundary of the continuum) is determined by the thermodynamic consistency condition proposed in [11]. The effect of the choice of ϵ_0 on the obtained degree of ionization is analyzed.

The rest of the paper is organized as follows. In Sect. 2 we briefly present the theoretical background; since the simple TF model is used throughout the paper for comparison with our AAM, this is introduced first (Sect. 2.1), whereas details of the RHFS implementation are presented in Sect. 2.2. Section 2.3 is devoted to discussion of the thermodynamic consistency condition. In Sect. 3 we present results of the model for Ar in a wide range of temperatures and densities. Conclusions are outlined in Sect. 4.

*corresponding author; e-mail: flanzini@exa.unicen.edu.ar

2. Theory

2.1. The generalized Thomas–Fermi model

The generalized Thomas-Fermi (TF) model [9, 11] treats the problem of a nucleus of charge Z positioned at $r = 0$, and Z electrons confined to the ion sphere, which results electrically neutral. The total nuclear+electronic potential is zero on and beyond the boundaries of the ion sphere. The model has, basically, two ingredients. The potential $V(r)$ due to the nucleus and the electrons is assumed spherically symmetric, and satisfies the Poisson equation [10]:

$$\nabla^2 V(r) = -4\pi\big(Z\delta(r) - \rho(r)\big), \tag{1}$$

where $\delta(r)$ is the Dirac delta function, and $\rho(r)$ is the electron density [†].

The second ingredient is that the number of electrons occupying a volume element $\mathrm{d}^3r\mathrm{d}^3p$ in phase space is given by the Fermi–Dirac distribution

$$n(\boldsymbol{r},\boldsymbol{p}) = \frac{1}{1+\exp\left(\frac{E-\mu}{T}\right)} = \frac{1}{1+\exp\left(\frac{p^2/2-V(\boldsymbol{r})-\mu}{T}\right)} \tag{2}$$

and then the electron density is given by

$$\rho(r) = \int n(\boldsymbol{r},\boldsymbol{p})\,\mathrm{d}^3\boldsymbol{p} = 4\pi\int n(r,p)p^2\,\mathrm{d}p = \frac{(2T)^{3/2}}{2\pi^2} I_{1/2}\left(\frac{V(r)+\mu}{T}\right), \tag{3}$$

where

$$I_k(x) = \int_0^\infty \frac{y^k\,\mathrm{d}y}{1+\exp(y-x)} \tag{4}$$

are the Fermi–Dirac integrals. In the previous expressions, T is temperature, measured in energy units, and μ is the chemical potential, obtained from the condition of charge neutrality within the ionic sphere

$$4\pi\int_0^{R_0}\rho(r)r^2\,\mathrm{d}r = Z$$

Combining Eqs. (1) and (3) results

$$\nabla^2 V(r) = -4\pi Z\delta(r) + \frac{2}{\pi}(2T)^{3/2} I_{1/2}\left(\frac{V(r)+\mu}{T}\right). \tag{5}$$

This equation is solved with the boundary conditions $V(R_0) = 0$, $(\mathrm{d}V/\mathrm{d}r)_{r=R_0} = 0$, and $rV(r)|_{r=0} = Z$, where R_0 is the radius of the spherical cell.

2.2. Average atom model

One of the greatest limitations of the generalized TF model is that it cannot account for the detailed shell structure of the bound electrons. For instance, for spectroscopic purposes, a quantum mechanical description of this shell structure is required. In order to overcome this problem, more detailed models treat separately the bound and the free electron densities

$$\rho(r) = \rho_b(r) + \rho_f(r). \tag{6}$$

In these models, the free electrons are generally treated statistically by means of the Fermi–Dirac distribution, in a similar fashion in which all the electrons are treated by the generalized TF model. The bound electron states are treated quantum mechanically by solving the Schrödinger or Dirac equations. In the AAM (see Refs. [11–13]), the occupation of the discrete ionic states are obtained as a by-product of the calculation from a statistical Fermi distribution, resulting in fractional, average, occupancies. In the following, we briefly present the treatment of the relativistic AAM due to Nikiforov and coworkers [11, 12].

In the relativistic approach we have, for the bound states

$$\rho_b(r) = \frac{1}{4\pi r^2}\sum_{\substack{n,l,j\\(\epsilon_{nlj}<\epsilon_0)}} N_{nlj}\left[F^2_{nlj}(r) + G^2_{nlj}(r)\right]. \tag{7}$$

Here,

$$N_{nlj} = \frac{2j+1}{1+\exp\left(\frac{\epsilon_{nlj}-\mu}{T}\right)} \tag{8}$$

represents the occupation of the electronic level according to the Fermi statistics. The numbers n, l, j, characterizing each single-electron level are the principal, the angular-momentum, and total-momentum quantum numbers, and ϵ_{nlj} is the corresponding eigenvalue; as above, μ is the chemical potential and T — the temperature. The summation is performed over the n, l, j levels whose eigenvalues ϵ_{nlj} are below a cut-off energy ϵ_0, which plays the role of an effective boundary of the continuum [11]. The functions $F_{nlj}(r)$ and $G_{nlj}(r)$ are the large and small radial components of the wave function multiplied by r. The radial wave functions and eigenenergies are determined by solving the radial Dirac equations [14, 15]. This can be done numerically, for instance, using the Numerov method [16]. In this work, however, the solution to the radial wave functions are approximated by means of hydrogenic solutions $F^H_{nlj}(r)$ and $G^H_{nlj}(r)$. These are the well-known analytical solutions to the Dirac equations for hydrogenic atoms, expressible in terms of Laguerre polynomials [14]. The only adjustable parameter in $F^H_{nlj}(r)$ and $G^H_{nlj}(r)$ is the effective (screened) charge Z_{nlj}; in order to determine its value, a minimization procedure is employed. In the method of the *trial potential*, the effective charge Z_{nlj} of each orbital n, l, j is found from the condition of minimum of the integral [12]:

$$J(Z_{nlj}) = \int_0^{R_0}\left[rV(r) - rV^H(r)\right]^2\left[\left(F^H_{nlj}\right)^2 + \left(G^H_{nlj}\right)^2\right]\mathrm{d}r, \tag{9}$$

[†]Here and in the following we employ atomic units, so $e = 1$, $m = 1$, $\hbar = 1$

where

$$V^H(r) = \frac{Z_{nlj}}{r} - A_{nlj}$$

and

$$A_{nlj} = \int_0^{R_0} \left[\frac{Z_{nlj}}{r} - V(r)\right] \left[\left(F^H_{nlj}\right)^2 + \left(G^H_{nlj}\right)^2\right] \mathrm{d}r.$$

Minimization of Eq. (9) was made, in the present implementation, by the method of *golden section search*.

The energy levels are given by

$$\epsilon^H_{nlj} = -\frac{Z^2_{nlj}/\widetilde{n}^2}{1 + \zeta^2\widetilde{n}^2 + \sqrt{1 + \zeta^2/\widetilde{n}^2}} + A_{nlj}, \tag{10}$$

where

$$\widetilde{n} = n - \frac{\zeta^2}{(j+1/2) + \sqrt{(j+1/2)^2 - \zeta^2}}$$

The second term in (6) is given by

$$\rho_f(r) = \frac{(2T)^{3/2}}{2\pi^2} \int_{y_0}^{\infty} \frac{y^{1/2} dy}{1 + \exp\left(y - \frac{V(r)+\mu}{T}\right)} = \tag{11}$$

$$\rho_f(r) = \frac{(2T)^{3/2}}{2\pi^2} \left[I_{1/2}\left(\frac{V(r)+\mu}{T}\right) - \int_0^{y_0} \frac{y^{1/2}\,\mathrm{d}y}{1 + \exp\left(y - \frac{V(r)+\mu}{T}\right)} \right], \tag{12}$$

where $y_0(r) = \max\left(0; \frac{V(r)+\epsilon_0}{T}\right)$; $I_{1/2}(x)$ is the Fermi–Dirac integral of Eq. (4). There are several different analytical approximations for $I_{1/2}(x)$, some of them defined only on reduced ranges of the argument values (see for instance [17]). In this work, the analytical approximation proposed in [18] is employed; this is valid in the whole range $-\infty < x < \infty$ with an error below 0.53%. Expression (12) is analogous to the expression for the full electron density obtained in the generalized TF approach (Eq. (3)), but now the bound states (those whose energy is below the threshold ϵ_0) are excluded from ρ_f. At this point, the present implementation differs from the one recently proposed by Kouser et al. [19], which employ a constant free electron density, equal to the electron density at the atomic shell boundary.

It should be noted that the model described so far constitutes a hybrid model, in the sense that the bound electrons are treated quantum mechanically and the free electrons by means of the non relativistic generalized TF approach. This is the case for most self-consistent methods [20]. A possible improvement can be obtained by employing, instead, the recently developed relativistic finite temperature Thomas–Fermi formalism [21, 22].

Expressions (7) and (11) depend both on the chemical potential μ and on the total potential $V(r)$. As in the TF model, the chemical potential is determined by the condition of charge neutrality inside the atomic sphere

$$4\pi \int_0^{R_0} (\rho_b(r) + \rho_f(r)) r^2\,\mathrm{d}r = Z \tag{13}$$

On the other hand, the Coulomb potential $V_C(r)$ depends on the electronic density itself, through a Poisson equation

$$\frac{1}{r}\frac{\mathrm{d}^2}{\mathrm{d}r^2}(rV_C) = 4\pi\left[\rho_b(r) + \rho_f(r)\right] \tag{14}$$

with the boundary conditions $|rV_C(r)|_{r=0} = Z$ and $V_C(R_0) = 0$. Equivalently,

$$V_C(r) = \frac{Z}{r} - 4\pi\left[\frac{1}{r}\int_0^r r'^2\rho(r')\,\mathrm{d}r' + \int_r^{R_0} r'\rho(r')\,\mathrm{d}r'\right] \tag{15}$$

Besides, in order to take into account the exchange effects, an exchange correction term $V_{ex}(r)$ is added to the potential [11]:

$$V_{ex}(r) = \frac{\pi\rho(r)}{T}\left[1 + 5.7\frac{\rho(r)}{T^{3/2}} + \frac{\pi^4}{3}\frac{\rho^2(r)}{T^3}\right]^{-1/3} \tag{16}$$

and the total potential is the sum of both terms

$$V(r) = V_C(r) + V_{ex}(r). \tag{17}$$

The above system of Eqs. (6)–(17) constitutes a complicated system of coupled equations. Since $\rho_b(r)$ and $\rho_f(r)$ depend on the potential $V(r)$ and this, in turns, depends on the density, the problem should be solved iteratively. As starting point for the iterative process, the values for $V^{(0)}(r)$ and $\mu^{(0)}$, as obtained within the generalized TF model, are used. After convergency is achieved, the values of the density $\rho(r)$, potential $V(r)$, chemical potential μ, radial wave functions $F_{nlj}(r)$ and $G_{nlj}(r)$, eigenenergies ϵ_{nlj}, and occupancies N_{nlj} of the bound states are obtained.

2.3. Thermodynamic consistency condition

The AAM described by Eqs. (6)–(17) rests in considering separately the free and bound electrons. The energy ϵ_0 appearing in Eqs. (7) and (12) acts as an effective boundary of the continuum separating those electrons considered as bounded, and treated quantum-mechanically, and those considered as free and treated with a semiclassical approach. The validity of different criteria for choosing the value of ϵ_0 is discussed, for instance, in Refs. [11, 23]. It is shown that an incorrect criterium leads to the appearance of unphysical discontinuities in the thermodynamic functions when they are evaluated in a range of temperatures and/or densities. This happens when discrete energetic levels of the bound states ϵ_{nlj} pass across ϵ_0 as T or ρ are varied.

A method to overcome this drawback is proposed in [11, 24]. The value of ϵ_0 is selected by a thermodynamic consistency condition (TCC), which is obtained after a variational procedure requiring that the bound states do not cross the value ϵ_0 for small variations of the occupation numbers and wave functions. The criterium can be summarized as

$$f_1(\epsilon_0) - f_2(\epsilon_0) = 0, \tag{18}$$

where

$$f_1(\epsilon_0) = \sum_{\substack{n,l,j \\ \epsilon_{nlj} < \epsilon_0}} (2j+1)$$

is the number of available bound states with eigenvalues below ϵ_0 and f_2 has the same meaning that f_1 in the semiclassical approximation

$$f_2(\epsilon_0) = \frac{8\sqrt{2}}{3\pi} \int_0^{R_0} [\max(0, \epsilon_0 + V(r))]^{3/2} r^2 \, \mathrm{d}r.$$

Whereas the funcion f_2 varies smoothly with ϵ_0, the function f_1 has a stepped behaviour. Consequently, Eq. (18) has, in general, several solutions. For studies of matter in wide ranges of temperatures and densities, condition (18) avoids sharp and unphysical changes on the derivatives of the free energy.

The introduction of the continuum threshold ϵ_0 was originally proposed for the AAM [11, 24], and later extended to a model based on the superconfiguration approximation by Pain [20].

It is important to note that the TCC described here corresponds to the case where the free electrons are treated non relativistically (Eq. (11)). If a relativistic approach is used instead, the condition for the determination of ϵ_0 may be different, since function $f_2(\epsilon_0)$ will change.

3. Results and discussion

3.1. Effective boundary of the continuum

We first present results regarding the selection of the energy ϵ_0 by the application of the thermodynamic consistency condition, Eq. (18). In Fig. 1, the variation of $f_1(\epsilon_0)$ and $f_2(\epsilon_0)$ for Ar with density $n_i = 2.2{\times}10^{22}$ cm^{-3} and different temperatures is shown. It can be seen that the TCC $f_1(\epsilon_0) = f_2(\epsilon_0)$ is satisfied not at a single point, but at different values of ϵ_0. In the figure, the corresponding values of f_1 and f_2 are indicated at the intersection points. These points correspond to integer values of $f_1 = f_2$ which are the number of available bound states with energies $\epsilon_{nlj} < \epsilon_0$. For instance, the solution $f_1 = f_2 = 10$ corresponds to a situation where the effective boundary of the continuum ϵ_0 is placed above the $1s$, $2s$, $2p_{1/2}$ and $2p_{3/2}$ levels (a total of 10 discrete available states), but below the eigenvalue of the $3s$ subshell. In the right axis of Fig. 1 the ionization degree Z_{free} obtained for the different values of ϵ_0 is also plotted.

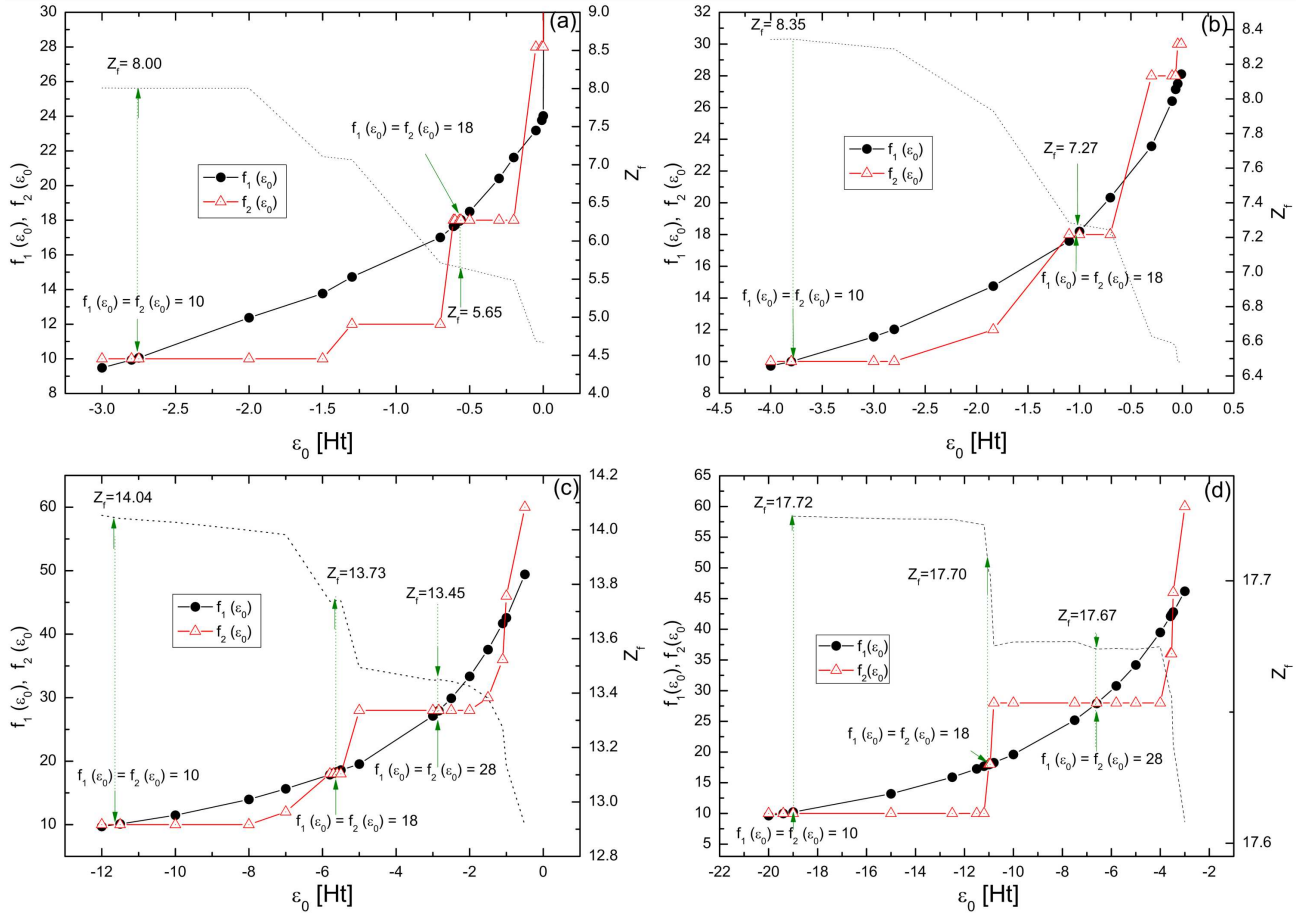

Fig. 1. Functions f_1 and f_2, and ionization degree Z_f against the cut-off energy ϵ_0 for Ar, with ionic density $n_i = 2.2 \times 10^{22}$ cm^{-3} and different temperatures: (a) $T = 25$ eV, (b) $T = 50$ eV, (c) $T = 200$ eV, (d) $T = 1000$ eV.

As pointed out in [11], at high temperatures the choice of ϵ_0 does not significantly alter the obtained electron density $\rho(r)$ nor the potential $V(r)$. This is reflected, for instance, in Fig. 1d: at $T = 1000$ eV three roots of Eq. (18) can be observed, namely $\epsilon_0^{(1)} \approx -19.4Ht$ ($f_1(\epsilon_0^{(1)}) = f_2(\epsilon_0^{(1)}) = 10$); $\epsilon_0^{(2)} \approx -10.95Ht$ ($f_1(\epsilon_0^{(2)}) = f_2(\epsilon_0^{(2)}) = 18$) and $\epsilon_0^{(3)} \approx -6.6Ht$ ($f_1(\epsilon_0^{(3)}) = f_2(\epsilon_0^{(3)}) = 28$). Despite the relative spread in the values of ϵ_0, the ionization degree takes almost the same value: $Z_f(\epsilon_0^{(1)}) = 17.72$; $Z_f(\epsilon_0^{(2)}) = 17.70$ and $Z_f(\epsilon_0^{(3)}) = 17.67$. This is due to the fact that levels with high quantum number (in this case, $n \geq 3$) are predicted to be practically unnocupied ($N_{nlj} \ll 1$). At lower temperatures, however, different choices of ϵ_0 lead to significantly different predictions for the ionization degree; in the extreme case of Fig. 1a, for $T = 25$ eV, the two roots of Eq. (18), which correspond to $f_1 = f_2 = 10$ and $f_1 = f_2 = 18$, imply $Z_f = 8.00$ and $Z_f = 5.65$, respectively. This difference arose because subshells with $n = 3$ have, at this temperature, non-negligible occupancies.

The above discussion shows the subtleties involved in the application of the thermodynamic consistency condition. It seems to be clear that, when studying the properties of matter in a range of temperatures and/or densities, the value of $f_1(\epsilon_0) = f_2(\epsilon_0)$ should remain the same; on the contrary, a number of discrete states will cross through ϵ_0 at some stage of the calculations. Secondly, the occupation N_{nlj} of bound states with $\epsilon_{nlj} > \epsilon_0$ should be small in all the range of interest. According to [11], the value of ϵ_0 should be selected in a way that, under normal conditions ($T = 0$, $\rho = \rho_0$, where ρ_0 is the normal density of matter) lies in the region of the upper level of electron energies (or in the conduction band for metals) (cf. [11], pages 308 and 319). Following this additional criterion, all the calculations presented below were performed at a value of ϵ_0 such that the condition $f_1(\epsilon_0) = f_2(\epsilon_0) = 18$ is satisfied.

3.2. Free charges

The effective boundary of the continuum discussed above is used as an input parameter in the RHFS calculations. Once the value of ϵ_0 has been established by using the TCC criterion, the self-consistent cycle is initiated. The ionization state is obtained after convergence of the self-consistent system of Eqs. (6)–(17). The number of free electrons Z_f can be obtained by integration of the free electron density, (11):

$$Z_f^{\mathrm{AAM}} = 4\pi \int_0^{R_0} \rho_f(r) r^2 \,\mathrm{d}r =$$

$$4\pi \int_0^{R_0} \left[\frac{(2T)^{3/2}}{2\pi^2} \int_{y_0}^{\infty} \frac{y^{1/2}\,\mathrm{d}y}{1 + \exp\left(y - \frac{V(r)+\mu}{T}\right)} \right] r^2 \,\mathrm{d}r \quad (19)$$

or, alternatively, because of the charge neutrality condition, Eq. (13),

$$Z_f^{\mathrm{AAM}} = Z - Z_b^{\mathrm{AAM}} = Z - \sum_{\substack{n,l,j \\ \epsilon_{nlj} < \epsilon_0}} N_{nlj} =$$

$$Z - \sum_{\substack{n,l,j \\ \epsilon_{nlj} < \epsilon_0}} \frac{2j+1}{1 + \exp\left(\frac{\epsilon_{nlj} - \mu}{T}\right)}. \quad (20)$$

Figure 2a–c shows the resulting degree of ionization of Ar as function of temperature and for three different ionic densities. We compare the results obtained within the AAM formalism with those obtained by the generalized TF approach

$$Z_f^{TF} = Z_f^{(1)} - Z_f^{(2)}$$

with (we skip the details of the calculations, see [11]):

$$Z_f^{(1)} = \frac{8\sqrt{2}}{\pi} \int_0^{R_0} r^2 \left[V(r)\right]^{3/2} \times \left[\int_1^{\infty} \frac{t^2\,\mathrm{d}t}{1 + \exp\left((t^2-1)\frac{V(r)}{T} - \frac{\mu}{T}\right)} \right] \mathrm{d}r, \quad (21)$$

$$Z_f^{(2)} = \frac{8\sqrt{2}}{\pi} \int_0^{R_0} \frac{r^2 \left[V(r)\right]^{3/2}}{(R_0/r)^2 - 1} \times \left[\int_0^{1} \frac{t^2\,\mathrm{d}t}{1 + \exp\left(\frac{1-t^2}{(R_0/r)^2-1}\frac{V(r)}{T} - \frac{\mu}{T}\right)} \right] \mathrm{d}r \quad (22)$$

and also with the approximative analytical formula developed by More [23] to fit the Thomas–Fermi result

$$Z_f^{\mathrm{More}} = \frac{Zx}{1 + x + \sqrt{1+2x}} \quad (23)$$

where

$$x = 14.3139 \left(R^C + Q_1^C\right)^{0.6624/C}; \quad R = \frac{\rho\left[\mathrm{g/cm^3}\right]}{ZA};$$

$$Q_1 = \left(0.003323 T_0^{0.9718} + 9.26148 \times 10^{-5} T_0^{3.10165}\right) \times R^{-\exp\left(-1.763 + 1.43175 T_F + 0.31546 T_F^7\right)};$$

$$T_0 = \frac{T\,[\mathrm{eV}]}{Z^{4/3}} T; \quad T_F = \frac{T_0}{1 + T_0}$$

and $C = -0.366667 T_F + 0.983333$

It can be seen that the three methods follow the same general trend, being the values predicted by AAM somewhat higher than those obtained by the other two methods. Due to its quantum-mechanical treatment of the bound states, the AAM ionization curves capture the shell structure of the atom. This is particularly noticeable in Fig. 2a, where two plateaus, one at $Z_f \approx 16$, and other at $Z_f \approx 8$ can be seen. This means that He-like and Ne-like ions are more stable, due to their closed shell structure. The shell effect seems to be less appreciable as the ionic density increases.

In Fig. 3 the results of our implementation for a ionic density $n_i = 2.2 \times 10^{22}$ cm^{-3} (solid density) are compared with recent calculations by Neumayer et al. [25] using the

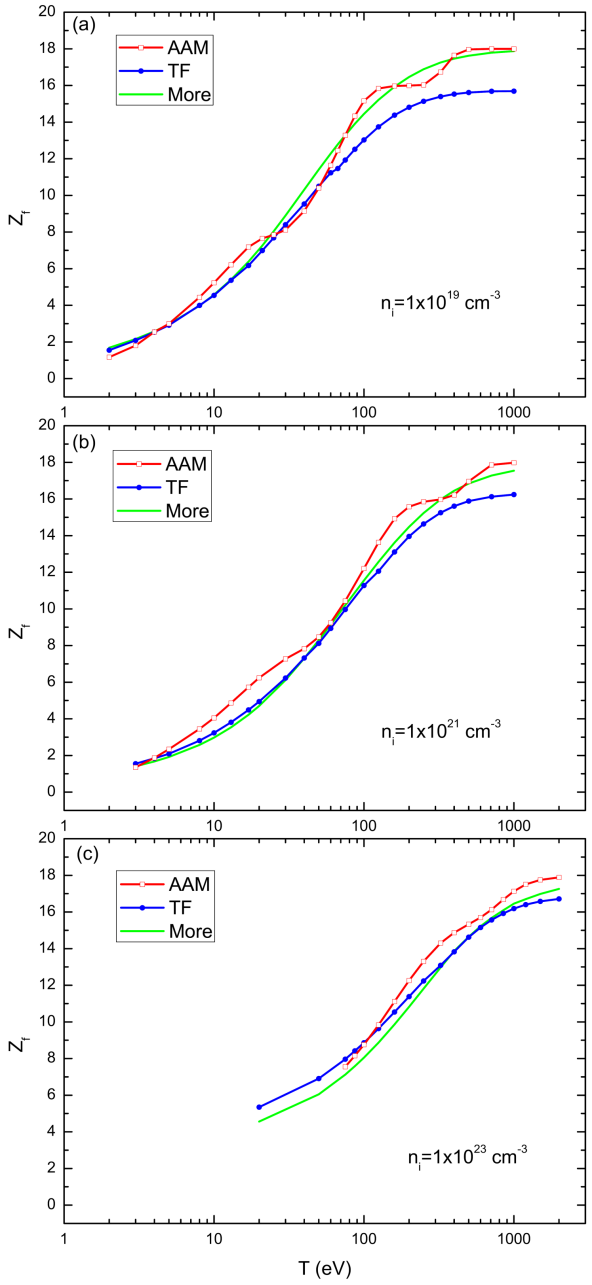

Fig. 2. Free charge Z_f for Ar at densities: (a) $n_i = 1 \times 10^{19}$ cm^{-3}, (b) $n_i = 1 \times 10^{21}$ cm^{-3}, (c) $n_i = 1 \times 10^{23}$ cm^{-3}.

collision-radiative code FLYCHK [26], and those by Sengebusch and coworkers [27]. The AAM implemented in this work predicts, in general, a higher ionization degree than the other two models. The difference can be attributed to the different types of treatments: the models in [25, 27] use a (more or less) detailed account of the ion distribution, whereas in the AAM a single, fictional average ion is considered. Our model predicts, for this density, a regular increment of Z_{free} with the temperature, in accordance with the FLYCHK results but contrasting with the results of [27], where a more stepped behaviour is observed.

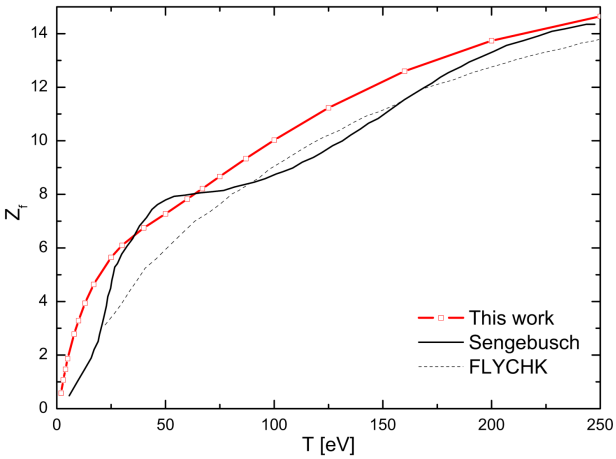

Fig. 3. Free charge Z_f for Ar with density $n_i = 2.2 \times 10^{22}$ cm^{-3} as obtained with the present implementation of the AAM, and comparison with the calculations of Refs. [25] and [27].

3.3. Electron density

Other output of the calculations is the electron density. In Fig. 4 we compare the radial distribution function $D(r) = 4\pi r^2 \rho(r)$ for $T = 10$, 50, and 200 eV and a ionic density $n_i = 1 \times 10^{19}$ cm^{-3}.

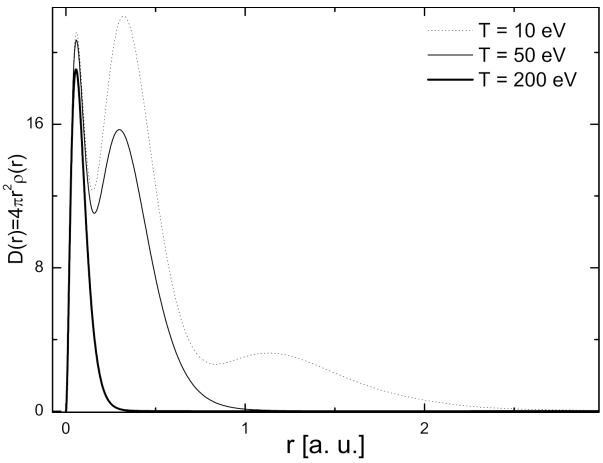

Fig. 4. Radial distribution density close to the nucleus for a ionic density $n_i = 1 \times 10^{19}$ cm^{-3} and three different temperatures: 10, 50, 200 eV.

As can be seen, the AAM correctly captures the shell structure of the atom; this is not feasible by the TF theory. Figure 4 shows the advance of ionization as the temperature increases: At $T = 10$ eV, the three lobes in $D(r)$ correspond, loosely speaking, to the $1s$, $2s+2p$, and $3s$ shells; at this temperature there are about 15 bound electrons (Fig. 2a); at $T = 50$ eV the $3s$ electrons have moved to the continuum, the corresponding lobe has disappeared; the number of bound electrons is around 8. Finally, at $T = 200$ eV, where $Z_f = 16$, only the $1s$ electrons remain bound.

Both in the TF model and in the AAM, the free electrons manifest as a long tail in the radial distribution function $D(r)$, extended to $r = R_0$. This is illustrated in Fig. 5 for $n_i = 1.0 \times 10^{19}$ cm^{-3} and $T = 200$ eV.

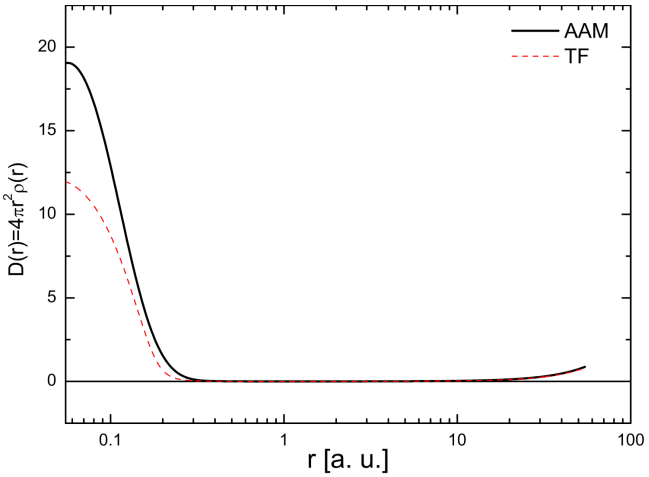

Fig. 5. Radial distribution function for $T = 200$ eV and $n_i = 1 \times 10^{19}$ cm^{-3}.

3.4. Contributions to the potential

By construction of the AAM, the potential $V(r)$ can be decomposed into several parts. First, the Coulombic potential $V_C(r)$ and the exchange correction term $V_{ex}(r)$ can be considered separately, Eq. (17); for V_{ex} we use the analytic approximation of Eq. (16). The Coulombic term can be, in turn, split into the nuclear attraction $V_N(r) = Z/r$ and the repulsive term due to all the other electrons $V_{el}(r)$ and which is given by the second, integral, term in Eq. (15). Besides, since in AAM the electron density is naturally separated in bound and free contributions, Eq. (6), the electronic part of the potential can be considered as consistent of two parts, $V_{el}(r) = V_{el,b}(r) + V_{el,f}(r)$, with

$$V_{el,i}(r) = -4\pi \left[\frac{1}{r} \int_0^r r'^2 \rho_i(r')\,\mathrm{d}r' + \int_r^{R_0} r' \rho_i(r')\,\mathrm{d}r' \right],$$

where $i = b,\ f$ stands for bound and free, respectively. The different contributions to the potential are plotted in Fig. 6a–c for $n_i = 1 \times 10^{19}$ cm^{-3}, and $T = 10$, 50, and 100 eV. It can be seen that the free electron contribution to the potential becomes more important as the temperature (and, correspondingly, the ionization degree) increases, whereas the bound electron contribution show the opposite behaviour. It should be noted that, as expected, at this low density the free electron part of the potential $V_{el,f}(r)$ can be well fitted by the expression for a uniform free-electron density [10]:

$$V_{el,f}(r) \approx \frac{3}{2}\frac{Z_f}{R_0}\left[1 - \frac{1}{3}\left(\frac{r}{R_0}\right)^2\right].$$

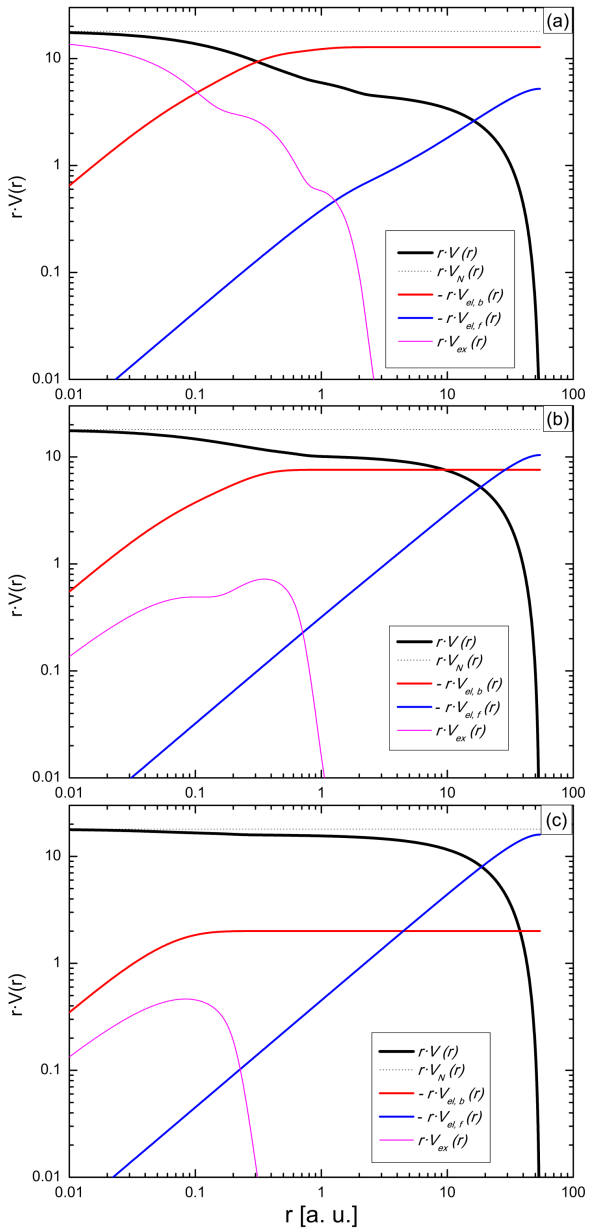

Fig. 6. Different contributions to the AAM potential for Ar with $n_i = 1 \times 10^{19}$ cm^{-3} and temperature (a) 10 eV, (b) 50 eV, (c) 200 eV.

4. Conclusions

We present an application of the average atom model for the calculation of properties of matter at high temperatures and densities. Some considerations regarding the computational implementation, particularly details about the choice of the effective boundary of the continuum are made. Satisfaction of the thermodynamic consistency condition is important to avoid discontinuities of the physical observables as they are analyzed as functions of temperature and/or density. We use Ar as a test case and analyze properties such as ionization degree, electron density, and contributions to the potential in a range of temperatures and densities.

Acknowledgments

The authors acknowledge the support of the Facultad de Ciencias Exactas, Universidad Nacional del Centro de la Provincia de Buenos Aires, and the Consejo Nacional de Investigaciones Científicas y Técnicas, Argentina.

References

[1] K.P. Driver, B. Militzer, *Phys. Rev. Lett.* **108**, 115502 (2012).

[2] Y. Hou, Y. Fu, R. Bredow, D. Kang, R. Redmer, J. Yuan, *High Energy Density Phys.* **22**, 21 (2017).

[3] W. Pei, T. Chang, *J. Quant. Spectrosc. Radiat. Transfer* **64**, 15 (2000).

[4] M.A. Mendoza, J.G. Rubiano, J.M. Gil, R. Rodríguez, R. Florido, G. Espinosa, P. Martel, E. Mínguez, *J. Quant. Spectrosc. Radiat. Transfer* **140**, 81 (2014).

[5] M.B. Trzhaskovskaya, V.K. Nikulin, *High Energy Density Phys.* **26**, 1 (2018).

[6] B.F. Rozsnyai, *High Energy Density Phys.* **10**, 16 (2014).

[7] L.H. Thomas, *Proc. Cambridge Philos. Soc.* **23**, 542 (1927).

[8] E. Fermi, *Rend. Accad. Naz. Lincei.* **6**, 602 (1927).

[9] R.P. Feynman, N. Metropolis, E. Teller, *Phys. Rev. B* **75**, 1561 (1949).

[10] D. Salzmann, *Atomic Physics in Hot Plasmas*, Oxford University Press, New York 1998.

[11] A.F. Nikiforov, V.G. Novikov, V.B. Uvarov, *Quantum-Statistical Models of Hot Dense Matter. Methods for Computation Opacity and Equation of State*, Birkhäuser Verlag, Basel 2005.

[12] A.F. Nikiforov, V.G. Novikov, A.D. Solomyannaya, *Laser and Particle Beams* **14**, 765 (1996).

[13] B.F. Rozsnyai, *Phys. Rev. A* **5**, 1137 (1972).

[14] M. Mizushima, *Quantum Mechanics of Atomic Structure and Atomic Spectra*, Benjamin, New York 1970.

[15] R.D. Cowan, *The Theory of Atomic Structure and Spectra*, University of California Press, Berkeley 1981 (revised October 2001).

[16] J.C. Slater, *The Calculation of Molecular Orbitals*, Wiley, USA 1979.

[17] O.N. Koroleva, A.V. Mazhukin, V.I. Mazhukin, P.V. Breslavskiy, *Math. Models Comput. Simulat.* **9**, 383 (2017).

[18] X. Aymerich-Humet, F. Serra-Mestres, J. Millán, *Solid State Electron.* **24**, 981 (1981).

[19] R. Kouser, G. Tasneem, M.S. Shahzad, S. Sardar, A. Ali, M.H. Nasim, M. Salahuddin, *Chin. Phys. B* **26**, 075201 (2017).

[20] J.C. Pain, *J. Phys. B At. Mol. Opt. Phys.* **40**, 1553 (2007).

[21] G. Faussurier, *Phys. Plasmas* **24**, 112901 (2017).

[22] M. Rotondo, J.A. Rueda, R. Ruffini, S.-S. Xue, *Phys. Rev. C* **83**, 045805 (2011).

[23] R.M. More, *Adv. At. Mol. Phys.* **21**, 305 (1985).

[24] G.V. Sin'ko, *High Temp.* **21**, 783 (1983); *Teplofiz. Vis. Temp.* **21**, 1041 (1983).

[25] P. Neumayer, B. Aurand, R.A. Costa Fraga, B. Ecker, R.E. Grisenti, A. Gumberidze, D.C. Hochhaus, A. Kalinin, M.C. Kaluza, T. Kühl, J. Polz, R. Reuschl, T. Stöhlker, D. Winters, N. Winters, Z. Yin, *Phys. Plasmas* **19**, 122708 (2012).

[26] H.-K. Chung, M. Chen, W.L. Morgan, Y. Ralchenko, R.W. Lee, *High Energy Density Phys.* **1**, 3 (2005).

[27] A. Sengebusch, H. Reinholz, G. Röpke, arXiv:arXiv:1709.08493v1, 2017.